the experimental results. Even more surprisingly, when the measured ρ_{xy} versus T curves shown in Fig. 1C are converted into the σ_{xy} versus M curves shown in Fig. 1D, they now all follow the same trend and match with our calculations. The curves are measured for different samples (with different saturation moments), but all follow the same rule qualitatively and could be simply explained by the reduction of M (*22*) (Fig. 1A). However, the comparison between the experiments and the calculations should be semi-quantitative, because the results are sensitive to the lattice structures. The calculated σ_{xy} for the fictitious cubic structure shows a strong deviation from that obtained for orthorhombic structure, and it changes the sign to be positive at low temperature (at large M). Therefore, more accurate information on the structure is needed to obtain the quantitative result. However, such a sensitivity does not affect our main results, i.e., the nonmonotonous behavior of σ_{xy}. Even the calculations for cubic structure show such behavior and may be used as a guide of possible deviation.

The results and analysis presented here should stimulate and urge the reconsideration of the electronic states in magnetic materials from a very fundamental viewpoint. For example, the MM is accompanied by the singularity of the vector potential, i.e., the Dirac string (*1*). As shown by Wu and Yang (*23*) this means that more than two overlapping regions have to be introduced, in each of which the gauge of the wave function is defined smoothly. This means that one cannot define the phase of the Bloch wave functions in a single-gauge choice when the MM is present in the crystal momentum space. This leads to some nontrivial consequences, such as the vortex in the superconducting order parameter as a function of $\mathbf{k}$ (*24*), and many others are left for future studies.

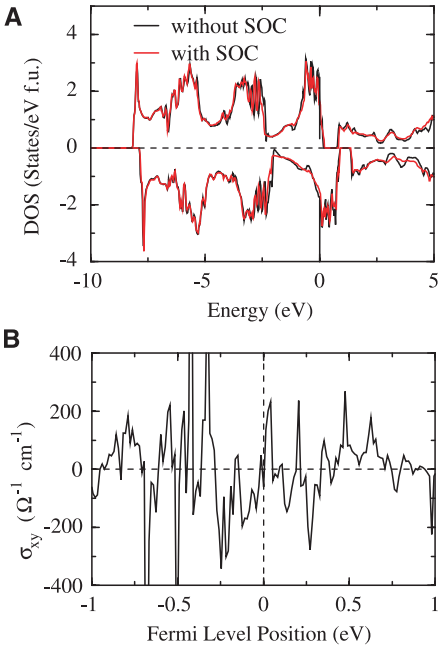

Fig. 4. The calculated (**A**) density of states (DOS) and (**B**) σ_{xy} as functions of Fermi-level position for the orthorhombic structure of single-crystal $SrRuO_3$. The Fermi level is shifted rigidly relative to the converged solution, which is specified as the zero point here. The sharp and spiky structure of σ_{xy} demonstrates the singular behavior of MMs. f.u., the formula unit $SrRuO_3$.

References and Notes

1. P. A. M. Dirac, *Proc. R. Soc. London* **133**, 60 (1931).
2. G. 't Hooft, *Nucl. Phys.* **B79**, 276 (1974).
3. A. M. Polyakov, *JETP Lett.* **20**, 194 (1974).
4. M. V. Berry, *Proc. R. Soc. London Ser. A* **392**, 45 (1984).
5. It has been recognized in the original paper by Berry (*25*) that the degeneracy point in the parameter space acts as a MM where the gauge field is enhanced.
6. H. Ohno, *Science* **281**, 951 (1998).
7. R. Karplus, J. M. Luttinger, *Phys. Rev.* **95**, 1154 (1954).
8. J. Smit, *Physica* **24**, 39 (1958).
9. W. Kohn, J. M. Luttinger, *Phys. Rev.* **108**, 590 (1957).
10. J. M. Luttinger, *Phys. Rev.* **112**, 739 (1958).
11. L. Berger, *Phys. Rev.* **B2**, 4559 (1970).
12. M. Onoda, N. Nagaosa, *Phys. Rev. Lett.* **90**, 206601 (2003).
13. T. Jungwirth, Q. Niu, A. H. MacDonald, *Phys. Rev. Lett.* **88**, 207208 (2002).
14. Y. Taguchi, Y. Oohara, H. Yoshizawa, N. Nagaosa, Y. Tokura, *Science* **291**, 2573 (2001).
15. J. Sinova, T. Jungwirth, J. Kucera, A. H. MacDonald, *Phys. Rev. B* **67**, 235203 (2003).
16. Materials and methods are available as supporting material on *Science* Online.
17. A. Shapere, F. Wilczek, *Geometric Phases in Physics* (World Scientific, Singapore, 1989).
18. D. J. Thouless, M. Kohmoto, M. P. Nightingale, M. den Nijs, *Phys. Rev. Lett.* **49**, 405 (1982).
19. R. M. Martin, *Phys. Rev. B* **5**, 1607 (1972).
20. R. D. King-Smith, D. Vanderbilt, *Phys. Rev. B* **47**, 1651 (1993).
21. This gauge field is distinct from that of the magnetic field $\boldsymbol{B}(\boldsymbol{r})$ in real space, although they are analogous to each other. In the presence of $\boldsymbol{B}(\boldsymbol{r})$, the covariant momentum operator π_μ is given by $\pi_\mu = -i\delta_{z\mu} + eA_\mu(\boldsymbol{r})$ where $\boldsymbol{B} = \nabla \times \boldsymbol{A}$. This leads to the commutation relation $[\pi_x, \pi_y] = -ie(\partial_x A_y - \partial_y A_x) = -ieB_z$, etc., and to the Lorenz force due to the magnetic field $\boldsymbol{B}$. Therefore, these two gauge fields, $b_\mu(\boldsymbol{k})$ and $\mathbf{B}(\mathbf{r})$, are dual to each other, and the presence of the one does not necessarily mean that of the other.
22. More Ca-doped samples with different concentrations have been measured. They all follow the same trend and are not shown here because of space limitations.
23. T. T. Wu, C. N. Yang, *Phys. Rev. D* **12**, 3845 (1975).
24. S. Murakami, N. Nagaosa, *Phys. Rev. Lett.* **90**, 057002 (2003).
25. M. Shikano, T. K. Huang, Y. Inaguma, M. Itoh, T. Nakamura, *Solid State Comm.* **90**, 115 (1994).

Supporting Online Material

www.sciencemag.org/cgi/content/full/302/5642/92/DC1
Materials and Methods
SOM Text
References and Notes

21 July 2003; accepted 28 August 2003

Coherent Soft X-ray Generation in the Water Window with Quasi–Phase Matching

Emily A. Gibson,[1] Ariel Paul,[1] Nick Wagner,[1] Ra'anan Tobey,[1] David Gaudiosi,[1] Sterling Backus,[1] Ivan P. Christov,[2] Andy Aquila,[3] Eric M. Gullikson,[3] David T. Attwood,[3,4] Margaret M. Murnane,[1] Henry C. Kapteyn[1]*

We demonstrate enhanced generation of coherent light in the "water window" region of the soft x-ray spectrum at 4.4 nanometers, using quasi–phase-matched frequency conversion of ultrafast laser pulses. By periodically modulating the diameter of a gas-filled hollow waveguide, the phase mismatch normally present between the laser light and the generated soft x-ray light can be partially compensated. This makes it possible to use neon gas as the nonlinear medium to coherently convert light up to the water window, illustrating that techniques of nonlinear optics can be applied effectively in the soft x-ray region of the spectrum. These results advance the prospects for compact coherent soft x-ray sources for applications in biomicroscopy and in chemical spectroscopy.

Coherent extreme ultraviolet (EUV) and soft x-ray light sources are of interest for applications in lithography, high-resolution imaging, site- and element-specific spectroscopy (*1*), and bio-microscopy (*2–4*). High harmonic generation (HHG) is a useful method for producing coherent, ultrafast, light in this region of the spectrum and can be implemented in a compact setup (*5–11*). In HHG, an intense ultrashort-pulse laser is focused into a gas or solid, generating high harmonics that emerge as a coherent, low-divergence beam (*12*). However, the conversion efficiency of the laser light to shorter wavelengths is limited by

[1]Department of Physics and JILA, University of Colorado, Boulder, CO 80309–0440, USA. [2]Department of Physics, Sofia University, Sofia, Bulgaria. [3]Center for X-ray Optics, Lawrence Berkeley National Laboratory, Berkeley, CA 94720, USA. [4]Applied Science and Technology, University of California, Berkeley, CA 94720, USA.

*To whom correspondence should be addressed. E-mail: kapteyn@jila.colorado.edu

difficulties in phase matching the frequency conversion process. The generation of higher order harmonics is accompanied by ionization of the gas medium. The resulting free-electron plasma causes a phase mismatch, allowing the laser light to "outrun" the generated light. Because the highest harmonics are generated at very high laser intensities after much of the gas has ionized, this phase mismatch limits the useful flux at the highest photon energies in the soft x-ray region of the spectrum. Overcoming this ionization-induced phase mismatch has thus been a critical challenge to the further development of coherent EUV and soft x-ray sources.

The conversion efficiency of laser light to high harmonics can be improved by focusing the fundamental laser light into a gas-filled hollow waveguide (*13*). Phase matching of the HHG conversion process can then be achieved by adjusting the gas pressure to balance the contributions to the phase velocity from the plasma and waveguide with that from the neutral gas. Because these contributions are of opposite sign, phase matching is possible at some pressure. The harmonic signal is then limited only by absorption. However, this method of phase matching can compensate only for relatively low levels of ionization (typically 0.5%, 1%, and 5% in He, Ne, and Ar) and has been demonstrated at photon energies <80 eV. At higher photon energies and ionization levels, the plasma contribution becomes much greater than the neutral gas contribution, making phase matching impossible. In the absence of phase matching, the harmonic emission builds up periodically over a coherence length and then interferes with out-of-phase light generated in the next section of the nonlinear medium.

By modulating the diameter of hollow-core waveguides with a periodicity of 0.5 to 1 mm, we previously demonstrated quasi–phase matching (QPM) of high harmonic generation, enhancing the conversion efficiency of harmonic photon energies up to 180 eV (*14*, *15*). The waveguide modulations create a periodic change in the intensity of the driving laser. Because both the spectrum and the phase of the generated EUV light depend very sensitively on the driving laser intensity, the waveguide modulations lead to phase and amplitude modulation of the EUV light, avoiding the otherwise inevitable destructive interference that limits the conversion efficiency. The phase-matched photon energies observed (~180 eV) were consistent with phase-matching HHG at ionization levels up to ~3% in He gas (2% and 8% in Ne and Ar). These ionization levels are still relatively low, however, and limit the highest photon energy at which QPM could be applied to 180 eV in He. Helium has the highest ionization potential of the noble gases and is therefore most difficult to ionize, allowing for the generation of higher harmonics at a relatively low ionization level. However, it also has the lowest effective nonlinear susceptibility and therefore emits relatively weak harmonics.

We present results that represent several advances in coherent soft x-ray technology. First, we demonstrate a phase-matching process that can operate in a fully ionized gas, allowing higher soft x-ray photon energies to be generated more efficiently. Second, we demonstrate that nonlinear optical phase-matching technologies can be applied to the generation of light in the scientifically and technologically important region of the spectrum around the carbon K absorption edge at 284 eV (4.4 nm). This energy range is important for biological and materials imaging, because water is transparent to soft x-ray radiation above 284 eV, whereas C atoms absorb this light. Third, we report water window coherent light generation with Ne gas as the nonlinear medium. Previous work had succeeded in generating only very small fluxes of light in the water window with He gas (*16*, *17*). The effective nonlinear susceptibility in HHG depends on the recollision cross section of an ionized electron with its parent ion; this cross section is smaller for He ions than for Ne. Fourth, this work shows that the light intensities required to reach the water window with HHG ($>10^{15}$ W cm^{-2}) can be reliably used in conjunction with a guided-wave geometry, which both permits quasi–phase matching and guides the high-intensity driving laser over many Rayleigh lengths. Finally, this work was done with an experimental setup that is simple and practical for applications, consisting of a small-scale (~2 m^2), high-repetition-rate laser system, together with a tabletop soft x-ray generation setup taking up ~0.2 m^2 of space.

In our experiment, we focused light from a 1 kHz Ti:sapphire laser system (*18*) producing 22-fs pulses, with a pulse energy of 1 to 3 mJ, into either a straight or modulated 150-μm inner diameter, 2.5-cm long, hollow-core waveguide filled with Ar or Ne gas. The modulations of the waveguide inner diameter are approximately sinusoidal, with a depth of ~10% and a period of 0.25 mm (Fig. 1). Care was taken to eliminate stray laser light and to accurately calibrate the EUV spectrometer (*19*).

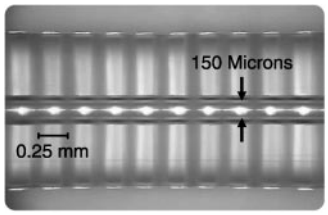

Fig. 1. Optical microscope image of a modulated hollow-core waveguide with a period of 0.25 mm and an inner diameter of 150 μm. The modulations were produced with glassblowing techniques in which a straight 150-μm inner diameter hollow-core fiber was pressurized and heated.

Harmonic spectra were obtained for 9 torr of Ne gas in modulated and straight waveguides, at a laser intensity of 1.6×10^{15} W cm^{-2} (Fig. 2A). At these intensities, a simple calculation of the expected cutoff harmonic energy (E_c) predicted by the rescattering model (*20*, *21*)—$E_c = I_p + 3.17U_p$, where $U_p \propto I_p\lambda^2$ is the ponderomotive potential, I_p is the ionization potential of Ne, and λ is the fundamental wavelength—yields an expected cutoff of 330 eV. However, the observable harmonic emission from the straight waveguide (Fig. 2A, black curve) only extends to at most 225 eV. In contrast, the harmonic emission from the 0.25-mm-period modulated waveguide (red curve) is brighter and extends to significantly higher energies, and the C edge at 284 eV is clearly visible.

The data of Fig. 2A illustrate that the highest observed harmonic orders are not limited by the $I_p + 3.17U_p$ relation, but by ionization-induced phase mismatch. The modulated waveguide compensates for this phase mismatch, making it possible to observe higher harmonics. By the peak of the laser pulse, calculations using the theory of Ammosov, Delone, and Krainov (ADK) (*22*,

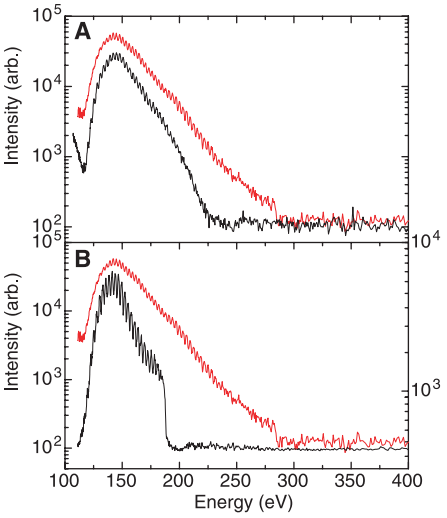

Fig. 2. (**A**) Harmonic emission from 9 torr of Ne in a straight (black) and a 0.25-mm-period modulated (red) waveguide, through Ag and C filters, at a laser intensity of 1.6×10^{15} W cm^{-2}, from harmonic order 73 (112 eV) to 183 (284 eV). The Ag filter is used to reject the laser light. The emission from the modulated waveguide extends to higher energies and is brighter than that from the straight guide. (**B**) Harmonic emission from 9 torr of Ne, taken under the same conditions as (A), with filters inserted for accurate energy calibration. Red curve, right axis: Ag and C filters, showing the C edge at 284 eV. Black curve, left axis: Ag and B filters to show the B edge at 188 eV.

23) and quantum calculations (*24*–*26*) indicate that Ne should be ~70 to 90% ionized, which is well above the level of ionization at which it has been possible in the past to demonstrate enhancement due to phase matching. The visibility of the harmonic peaks is limited by the finite resolution of the spectrometer, convolved with the width of the harmonics themselves, which is influenced by both intrinsic (*27*) and ionization-induced phase shifts at these high intensities and ionization levels (*28*). With He gas, the signal levels were about one-tenth as high, and we were not able to observe light at the C edge from He because of lower signal-to-noise ratios. Although past work observed HHG from He in the water window, this process was not phase matched and therefore produced significantly lower signal levels and thus required higher laser energies or higher sensitivity detection (*16*, *17*).

Harmonic emission is shown (Fig. 3) for Ar in 2.5-cm-long straight and modulated waveguides, at a lower peak intensity of 9×10^{14} W cm^{-2}. At this intensity, Ar is fully ionized by the peak of the pulse, and substantial double ionization is present. Even at these very high ionization levels, the modulated waveguide increases the HHG flux over the entire energy range, by up to a factor of 3 at the highest enhancements. We observed HHG up to photon energies of ~175 eV in both straight and modulated waveguides, corresponding to the expected harmonic cutoff for the laser intensity used. Previously, the highest harmonic observed with Ar was 100 eV with an 800 nm driving laser (even with 7-fs driving pulses, or ~100 mJ pulse energies) (*20*, *29*, *30*). We believe that the hollow-waveguide geometry limits plasma-induced laser beam defocusing, making it possible to generate very high harmonics.

The different regimes of signal enhancement observed in both Ne and Ar gas with modulated waveguides are consistent with high-order quasi–phase matching of HHG. Using either the ADK or a fully quantum tunneling model, we calculate the level of ionization present for a given harmonic generated by our laser pulse. Knowing this value, we then calculate the phase mismatch between the fundamental and the qth harmonic, $\Delta k = k_q - qk_f$, due to the waveguide, plasma, and neutral atoms (*13*, *30*)

$$\Delta k_{\text{total}} = \Delta k_{\text{guide}} + \Delta k_{\text{plasma}} + \Delta k_{\text{neutrals}} \quad (1)$$

or

$$\Delta k = \frac{q u_{11}^2 \lambda}{4\pi a^2} + P\eta N_{atm} r_e (q\lambda - \lambda/q) - \frac{2\pi(1-\eta)Pq}{\lambda}(\delta(\lambda) - \delta(\lambda/q)) \quad (2)$$

where λ, q, a, u_{11}, η, P, N_{atm}, r_e, and δ are the fundamental wavelength, harmonic order, waveguide radius, first zero of the Bessel function J_0, ionization fraction, gas pressure in atmospheres, number density at 1 atm, classical electron radius, and index of refraction of the neutral gas at 1 atm, respectively. Under the conditions of low pressure and high ionization, the contribution of the neutral gas to the phase mismatch can be neglected, and the dominant term in Eq. 2 is due to the plasma. To a first approximation, $\Delta k_{\text{plasma}} \sim P\eta N_{\text{atm}} r_e q\lambda = q\omega_p^2/2c\omega$. From this approximation, we calculate $\Delta k \sim 90{,}000$ m^{-1} for the harmonics at the C edge in Ne, 183rd order (284 eV) at ~60% ionization. For the 109th order in Ar (~170 eV) in fully ionized Ar with some double ionization, we calculate $\Delta k \sim 80{,}000$ m^{-1}, whereas for the plateau harmonics around harmonic order 71 (~110eV), $\Delta k \sim 20{,}000$ m^{-1}.

This phase mismatch can be compensated for by the modulated waveguide. In a simplified model of harmonic generation, the field of harmonic order q after propagating a distance L in a nonlinear medium is related to the phase mismatch,Δk, by

$$E_q \propto \int_0^L E_\omega^n(z) d(z) e^{-i\Delta k z} dz \quad (3)$$

where E_ω is the fundamental field, n is the effective order of the nonlinear process, $d(z)$ is the nonlinear coefficient, and Δk is the phase mismatch calculated above. In our case, the nonlinear coefficient can be expressed as a general periodic function of z with period Λ (*31*)

$$d(z) = \sum_{m=-\infty}^{\infty} D_m e^{iK_m z} \quad (4)$$

where $K_m = 2\pi m/\Lambda$, Λ is the modulation period of the quasi–phase matching (i.e., 0.25 mm), and m is the order of the QPM process. Eqs. 3 and 4 show that the harmonic signal will be enhanced when $K_m \approx \Delta k$. The enhancement in signal will be greatest for $m = 1$, but QPM will still enhance the HHG signal for higher values of m. For example, for a waveguide with a 0.25-mm periodicity, $K_1 = 25{,}400$ m^{-1}. This value agrees well with the phase mismatch calculated for the midplateau harmonics in Ar (i.e., $\Delta k \sim 20{,}000$ m^{-1}), where we observe the greatest enhancement. The calculated phase mismatch of $\Delta k \sim 80{,}000$ m^{-1} for the cutoff harmonics in Ar at 175 eV is too great to be compensated in the case of $m = 1$; however, a higher order ($m = 3$) QPM process can enhance the signal. Third-order QPM corresponds to a case in which the HHG signal will rise, fall, and then rise again during the course of one half-period of the modulation. Therefore, we still observe an enhanced signal in the cutoff region in Ar. Finally, for the harmonics in Ne near the C edge at 284 eV, the large phase mismatch of ~90,000 m^{-1} can be compensated for with third- or fifth-order ($m = 3, 5$) QPM. In the case of these cutoff harmonics in Ne, the phase mismatch above 225 eV is so great that they can only be observed with a modulated waveguide and are not seen in a straight waveguide.

The ionization level is changing as a function of time during the laser pulse. Thus, at some point during the rising edge of the pulse, the phase mismatch will equal the effective k-vector for QPM for a large range of harmonic orders. This explains why many harmonic orders are enhanced by QPM, even though the periodicity and gas pressure are fixed. For a given harmonic order, the enhancement may also be due to different QPM orders at different times during the laser pulse. A complete picture of the QPM process should therefore take these dynamics into account.

The flux at these high energies is yet to be fully optimized. Currently, we can fabricate waveguides only 2.5 cm long with 0.25 mm periodicity. This means that we can access only high-order (i.e., m = 3, 5) QPM for the water-window region of the spectrum in a limited interaction length. On the basis of conservative estimates of detection efficiency, filter transmission, and measurements of grating efficiency, we determined a minimum flux of between 10^6 and 10^8 photons s^{-1} in a 10% bandwidth at the C edge. This corresponds to an estimated focusable intensity of 10^{11} to 10^{14} W cm^{-2}, assuming a pulse duration of 5 fs and a focused spot size of 20 nm with a 10% energy transmission optic, or alternatively, a peak and average spectral brilliance of $\sim 10^{21}$ and 10^{10} photons s^{-1} mm^{-2} mrad^{-2} per 0.1% bandwidth, respectively. This flux may be sufficient for biological imaging applications, and a number of improvements should further increase it. Thus, there is a clear path to pursue for implementation of a tabletop soft x-ray mi-

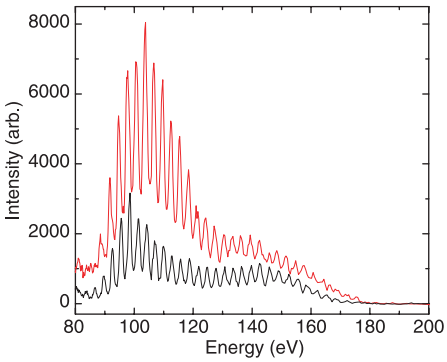

Fig. 3. Harmonic emission from a straight (black) and 0.25-mm-period modulated (red) waveguide filled with low-pressure Ar (7 torr), at a peak laser intensity of 9×10^{14} W cm^{-2}. A Zr filter was used to reject the laser light in this case. The emission extends from harmonic order 89 (80 eV) to 115 (180 eV).

croscope. Longer modulated waveguides with shorter modulation periods should significantly enhance the signal for several reasons. First, $m = 1$ QPM should become possible by using shorter periods. Second, the 2.5-cm modulated waveguide length corresponds to only 0.3 absorption depths in Ne at 284 eV. Previous theoretical studies have indicated that 5 to 10 absorption depths are ideal for generating a maximum signal (*32*). Furthermore, because the highest HHG photon energy scales linearly with laser intensity, using very reasonable laser parameters (i.e., pulsewidth ~10 fs, intensities $\sim 5 \times 10^{15}$ W cm^{-2}) and waveguides with 0.1 mm periodicity, we should be able to generate high-order quasi–phase-matched light at photon energies approaching 1 keV.

References and Notes

1. R. Schoenlein *et al.*, *Science* **287**, 2237 (2000).
2. D. Attwood, *Phys. Today* **45**, 24 (August, 1992).
3. C. Jacobsen, *Trends Cell Biol.* **9**, 44 (1999).
4. G. Schneider *et al.*, *Surf. Rev. Lett.* **9**, 177 (February, 2002).
5. A. McPherson *et al.*, *JOSA B* **4**, 595 (1987).
6. M. Ferray *et al.*, *J. Phys. B* **21**, L31 (1987).
7. J. J. Macklin, J. D. Kmetec, C. L. Gordon, III, *Phys. Rev. Lett.* **70**, 766 (1993).
8. R. Haight, P. F. Seidler, *Appl. Phys. Lett.* **65**, 517 (1994).
9. D. Descamps *et al.*, *Opt. Lett.* **25**, 135 (2000).
10. M. Bauer *et al.*, *Phys. Rev. Lett.* **8702**, 5501 (2001).
11. L. Nugent-Glandorf, M. Scheer, D. Samuels, V. Bierbaum, S. Leone, *J. Chem. Phys.* **117**, 6108 (2002).
12. R. A. Bartels *et al.*, *Science* **297**, 376 (2002).
13. A. Rundquist *et al.*, *Science* **280**, 1412 (1998).
14. A. Paul *et al.*, *Nature* **421**, 51 (2003).
15. I. P. Christov, H. C. Kapteyn, M. M. Murnane, *Optics Express* **7**, 362 (2000).
16. Z. H. Chang, A. Rundquist, H. W. Wang, M. M. Murnane, H. C. Kapteyn, *Phys. Rev. Lett.* **79**, 2967 (1997).
17. C. Spielmann *et al.*, *Science* **278**, 661 (1997).
18. S. Backus, C. G. I. Durfee, G. A. Mourou, H. C. Kapteyn, M. M. Murnane, *Opt. Lett.* **22**, 1256 (1997).
19. The harmonic emission emerging from the waveguide passes through Zr or Ag filters (0.4 μm) to block the fundamental light, and the harmonics are then spectrally dispersed onto an Andor CCD camera with a Hettrick EUV spectrometer. The energy calibration of the spectrometer was verified by recording the positions of the Si, B, and C absorption edges, at 99.9 eV, 188.35 eV, and 284 eV, respectively.
20. C. G. Wahlström *et al.*, *Phys. Rev. A* **48**, 4709 (1993).
21. K. C. Kulander, K. J. Schafer, J. L. Krause, in *Super-Intense Laser-Atom Physics*, B. Piraux, A. L'Huillier, K. Rzazewski, Eds. (Plenum, New York, 1993), vol. 316, pp. 95–110.
22. M. V. Ammosov, N. B. Delone, V. P. Krainov, *Soviet Physics JETP* **64**, 1191 (1986).
23. V. P. Krainov, *JOSA B* **14**, 425 (1997).
24. I. P. Christov, M. M. Murnane, H. C. Kapteyn, *Phys. Rev. Lett.* **78**, 1251 (1997).
25. I. P. Christov, M. M. Murnane, H. C. Kapteyn, *Phys. Rev. A* **57**, R2285 (1998).
26. A. Scrinzi, M. Geissler, T. Brabec, *Phys. Rev. Lett.* **83**, 706 (1999).
27. Z. Chang *et al.*, *Phys. Rev. A* **58**, R30 (1998).
28. H. J. Shin *et al.*, *Phys. Rev. A* **63**, 053407 (2001).
29. M. Schnürer *et al.*, *Phys. Rev. Lett.* **83**, 722 (1999).
30. J. Zhou, J. Peatross, M. M. Murnane, H. C. Kapteyn, I. P. Christov, *Phys. Rev. Lett.* **76**, 752 (1996).
31. M. M. Fejer, G. A. Magel, D. H. Jundt, R. L. Byer, *IEEE J. Quantum Electron.* **28**, 2631 (1992).
32. E. Constant *et al.*, *Phys. Rev. Lett.* **82**, 1668 (1999).

33. This work was supported by the National Science Foundation and the Department of Energy and made use of facilities funded by the W. M. Keck Foundation.

1 July 2003; accepted 3 September 2003

Vibrational Mode–Specific Reaction of Methane on a Nickel Surface

Rainer D. Beck,* Plinio Maroni, Dimitrios C. Papageorgopoulos, Tung T. Dang, Mathieu P. Schmid, Thomas R. Rizzo

The dissociation of methane on a nickel catalyst is a key step in steam reforming of natural gas for hydrogen production. Despite substantial effort in both experiment and theory, there is still no atomic-scale description of this important gas-surface reaction. We report quantum state–resolved studies, using pulsed laser and molecular beam techniques, of vibrationally excited methane reacting on the nickel (100) surface. For doubly deuterated methane (CD_2H_2), we observed that the reaction probability with two quanta of excitation in one C-H bond was greater (by as much as a factor of 5) than with one quantum in each of two C-H bonds. These results clearly exclude the possibility of statistical models correctly describing the mechanism of this process and attest to the importance of full-dimensional calculations of the reaction dynamics.

The reaction of methane on a nickel catalyst to form surface-bound methyl and hydrogen is the rate-limiting step in steam reforming, which is the principal process for industrial hydrogen production as well as the starting point for the large-scale synthesis of many important chemicals such as ammonia, methanol, and higher hydrocarbons (*1*). Because of its importance, the dissociation of methane on nickel has been considered a prototype for chemical bond formation between a polyatomic molecule and a solid surface, with many experimental and theoretical studies directed at elucidating its mechanism (*2–14*). In view of the enormous economic importance of this process (*15*), it would be desirable to have a reliable theoretical description that could guide the development of improved catalysts (*2, 3*). Despite intense effort, there is still no atomic-scale picture of the dynamics of this important gas-surface reaction.

Molecular beam experiments (*4–6*) have firmly established that methane chemisorption is a direct process that can be activated with about equal efficiency by both incident kinetic energy normal to the surface and thermal vibrational energy of the incident methane. State-resolved reactivity measurements that used laser excitation of the asymmetric stretch fundamental vibration (ν_3) (*7*) and first overtone ($2\nu_3$) (*8*) of CH_4 incident on Ni(100) have confirmed the notion that vibrational energy is similar to translational excitation in its efficiency in promoting this reaction. Theoretical treatments of methane chemisorption have included wave packet simulations with up to nine vibrational degrees of freedom (*9*), reduced-dimensionality dynamical models with only a single C-H stretch vibration (*10–12*), and a greatly simplified statistical model (*13*). Despite having diametrically opposed presuppositions, both dynamical and statistical approaches claim to reproduce existing experimental data (*10, 16*), although they make different predictions about the role of methane vibrational excitation in promoting the reaction. Some dynamical calculations suggest that the reactivity of vibrationally excited methane on nickel should depend on the precise nature of the vibrational mode (*9, 17*), whereas statistical models predict the complete absence of such effects (*16*). Although the reverse process—the associative desorption of methane from transition metal surfaces—seems to deviate somewhat from a purely statistical model (*18, 19*), the experimental results reported thus far do not exclude either approach, because there is no reported evidence for mode specificity in the surface reaction of methane.

In contrast, mode-specific reactivity of methane in the gas phase has been observed. Yoon *et al.* (*20*) have found that when methane is excited to the symmetric stretch-bend combination $\nu_1 + \nu_4$, it is more reactive with atomic chlorine (by a factor of 1.9) than when it is promoted to the nearly isoenergetic antisymmetric combination $\nu_3 + \nu_4$. In a similar study, Kim *et al.* (*21*) observed that the product state distribution for the reaction of CD_2H_2 with chlorine depends on the initially

Laboratoire Chimie Physique Moléculaire, Ecole Polytechnique Fédérale de Lausanne (EPFL), CH-1015 Lausanne, Switzerland.

*To whom correspondence should be addressed. E-mail: rainer.beck@epfl.ch